International Journal of Heat and Mass Transfer 55 (2012) 3366–3378

Contents lists available at SciVerse ScienceDirect

International Journal of Heat and Mass Transfer

journal homepage: www.elsevier.com/locate/ijhmt

The effect of porous media particle size on forced convection from a circular cylinder without assuming local thermal equilibrium between phases

Gazy F. Al-Sumaily [a,*], Akira Nakayama [b], John Sheridan [a], Mark C. Thompson [a]

[a] Fluids Laboratory for Aeronautical and Industrial Research (FLAIR), Department of Mechanical and Aerospace Engineering, Monash University, Victoria 3800, Australia
[b] Department of Mechanical Engineering, Shizuoka University, 3-5-1 Johoku, Hamamatsu 432-8561, Japan

ARTICLE INFO

Article history:
Available online 10 April 2012

Keywords:
Forced convection
Porous media
Non-Darcian effects
Local thermal non-equilibrium
Particle diameter

ABSTRACT

A detail numerical analysis of the effect of particle diameter of a packed bed of spherical particles on forced convection about an embedded circular cylinder is presented. This parametric study focusses on the two-phase energy (*LTNE*—local thermal non-equilibrium) model, which does not assume local thermal equilibrium (*LTE*) between the solid medium and the fluid. The investigation is performed for a cylinder-to-particle diameter ratio $D_{cy}/d_p = 10–100$, at a wide ranges of Reynolds number $Re_D = 1–250$ and solid-to-fluid thermal conductivity ratio $k_r = 0.01–1000$. A comparison of predictions from the *LTNE* and *LTE* energy models is also made. This paper quantifies the influence of the key non-dimensional parameters on the heat transfer rate. It is also shown that although the presence of the porous materials around the heated cylinder enhances the overall heat transfer and increases the pressure drop in the bed compared to an empty channel, using a porous medium with large particle diameters increases considerably this enhancement in heat transfer and decreases significantly the unfavorable pressure drop.

1. Introduction

Forced convection heat transfer in porous media has many important applications in packed-bed reactors, catalytic and chemical particle beds, solid-matrix heat exchangers, packed-bed regenerators, and fixed-bed nuclear propulsion systems. Extensive studies of forced convective heat transfer and fluid flow in porous media have been reported in reviews provided by, for example, Ingham and Pop [18], Vafai [48], and Nield and Bejan [38].

Porous media can be used as an effective heat transfer augmentation technique. Porous structures intensify the mixing of the flowing fluid and increase the contact surface area and consequently enhance the convective heat transfer. Cooling systems using porous structures have been widely applied to cool microelectronic chips, i.e., see Kuo and Tien [28], and Chrysler and Simons [12]. Kuo and Tien suggested the use of a foam metal to enhance convective heat transfer from microelectronic chips, while Chrysler and Simons suggested the use of packed beds of spherical particles for the same application. Jeigarnik et al. [19], who experimentally examined forced convective heat transfer of water on flat plates and in channels filled with metallic porous materials, pointed out that the porous media may increase the heat transfer coefficient (5–10) times relative to an empty channel. Increased cooling efficiencies are becoming progressively more important as computer CPU units continue to increase the heat output. Nasr et al. [36] also experimentally investigated forced convection but this time of air from a circular cylinder embedded in a packed bed of spheres, demonstrating that the bed increases substantially the Nusselt number (up to seven times for aluminum spheres). Jiang et al. [23,25] studied numerically and experimentally forced convection heat transfer of water in a non-sintered porous vertical annulus and a horizontal plate channel. They found that the packed beds greatly intensify the convective heat transfer by up to 10 times.

Recently, the influence of the non-Darcian effects of variable porosity, variable thermo-physical properties, and thermal dispersion in a porous medium on heat transfer have been more widely studied in the literature. A comprehensive review of heat and flow characteristics in packed beds was published by Achenbach [1]. However, there are some seemingly contradictory conclusions concerning the dependence of the convective heat transfer on the porous structure, in particular, the particle diameter. In the works of Kwendakwema and Boehm [32], Wang and Du [52], David and Cheng [13], Jiang et al. [24,23] and Hsiao et al. [16], it was found that the heat transfer increases as the particle diameter increases. For instance, Kwendakwema and Boehm performed a numerical study to evaluate mixed convective heat transfer in a porous medium between two vertical concentric cylinders for constant temperature outer and insulated inner boundary conditions. In their flow simulations, the simple Darcy model was used, while the

* Corresponding author.
E-mail addresses: gazy.alsumaily@monash.edu (G.F. Al-Sumaily), tmanaka@eng.shizuoka.ac.jp (A. Nakayama), john.sheridan@monash.edu (J. Sheridan), mark.thompson@monash.edu (M.C. Thompson).

0017-9310/$ - see front matter © 2012 Elsevier Ltd. All rights reserved.
http://dx.doi.org/10.1016/j.ijheatmasstransfer.2012.03.007

Nomenclature

a_{sf}	specific interfacial area (m^{-1})
Bi	Biot number, $Bi = h_{sf} a_{sf} D_{cy}^2 / k_s$
c_p	specific heat capacity (J/kg K)
d_p	particle diameter (m)
D_{cy}	cylinder diameter (m)
Da	Darcy number, $Da = K/D_{cy}^2$
F	geometric function, $F = 1.75/\sqrt{150\varepsilon^3}$
h_{cy}	cylinder surface heat transfer coefficient (W/m^2 K)
h_{sf}	interfacial heat transfer coefficient (W/m^2 K)
H	channel height (m)
k	thermal conductivity (W/m K)
k_r	solid/fluid thermal conductivity ratio, $k_r = k_s/k_f$
K	permeability of the porous medium, $K = \varepsilon^3 d_p^2/150(1-\varepsilon)^2$ (m^2)
L	channel length (m)
Nu	time-mean average Nusselt number
p	Lagrangian polynomial order
$\acute{P}_f$	fluid pressure (N/m^2)
P_f	dimensionless fluid pressure
Pr	Prandtl number, $Pr = \nu_f/\alpha_f$
Re_D	Reynolds number, $Re_D = u_o \rho_f D_{cy}/\mu_f$
$\acute{t}$	time (s)
t	dimensionless time
$\acute{T}$	temperature (K)
$\mathbf{\acute{u}}$	vectorial fluid velocity (m/s)
$\mathbf{u}$	dimensionless vectorial fluid velocity, $\mathbf{u} = \mathbf{\acute{u}}/u_o$
$\acute{u}$	horizontal velocity component (m/s)
u	dimensionless horizontal velocity component
u_o	inlet horizontal fluid velocity (m/s)
$\acute{v}$	vertical velocity component (m/s)
v	dimensionless vertical velocity component
$\acute{x}, \acute{y}$	horizontal and vertical coordinates (m)
x, y	dimensionless horizontal and vertical coordinates

Greek symbols

α_r	solid-to-fluid thermal diffusivity ratio, $\alpha_r = \alpha_s/\alpha_f$
ε	porosity
θ	dimensionless temperature, $\theta = (\acute{T} - T_o)/(T_h - T_o)$
μ_f	fluid dynamic viscosity (kg/m s)
ρ_f	fluid density (kg/m^3)
φ	angular coordinate, (°)

Subscripts

eff	effective
f	fluid
o	inlet of the channel
out	outlet of the channel
s	solid
t	total

single-phase energy model was used to predict the thermal field. Wang and Du conducted their experiments on forced convection of water or transformer-oil flowing upward through a vertical annulus filled with glass beads.

However, Jeigarnik et al. [19], Nasr et al. [36], Hwang and Chao [17], Chen and Hadim [10], Jiang et al. [22] and Saito and Lemos [46] have found the opposite behavior. The main reason for this initially contradictory conclusion is the difference between the values of thermal conductivities of the solid and fluid phase, as explained by Jiang et al. [23]. They pointed out that when the solid thermal conductivity is much higher than that of the fluid, the heat transfer coefficient on the heated wall is mainly governed by direct conduction throughout solid particles. Therefore, when the particle diameter increases the contact surface between the wall and particles decreases, and consequently the heat transfer coefficient decreases. However, when these conductivities are of the same order, the heat transfer from the wall is controlled by convection, and when the particle diameter increases, the thermal dispersion increases, and this intensifies the convective heat transfer.

Others such as Jiang et al. [21,25] have developed a third conclusion which attributes the different behavior to a non-linear effect of the particle diameter on the convective heat transfer. They found that the convective heat transfer coefficient can decrease or increase as the particle diameter increases depending on the values of the mass flow rate, porosity, thermal dispersion effect, and solid and fluid thermal conductivities. Jiang et al. [21] examined numerically forced convection in a horizontal plate channel filled with solid metallic particles heated from the top wall by constant heat flux. The same physical problem was tested experimentally by Jiang et al. [25]. They used different solid materials, i.e., glass, stainless steel, and bronze, with water as the working fluid. The experimental results showed that the wall heat transfer coefficient increases with increasing the particle diameter for the channel with glass beads; however, the opposite result was found for the channel filled with stainless steel or bronze at different mass flow rates. They attributed the opposite trend to result from the competing factors of the thermal dispersion *(mixing effect)* and the decreased contact surface area between particles as the particle diameter increases. However, none of the preceding studies have systematically investigated the combined effects of interfacial heat transfer coefficient and particle diameter on convective heat transfer.

From the energy point of view, there are two different thermal models used in theoretical and numerical research: the *Local Thermal Equilibrium* (*LTE*) model and the *Local Thermal Non-Equilibrium* (*LTNE*) model. It has been established that the *LTE* model for convection in porous media, which assumes thermal equilibrium between the solid and fluid phases, is not necessarily a good approximation depending on problem parameters. This has been reported by various authors, for example by Vafai and Sozen [49], Kaviany [27] and Pop and Cheng [39]. As such, more recently more attention has been paid to the *LTNE* model to provide more physically realistic and accurate predictions of convection heat transfer processes in porous media. Representative works, for related problems of convection and for different applications include Carbonell and Whitaker [9], Vafai and Sozen [49], Quintard and Whitaker [41], Amiri and Vafai [3], Amiri et al. [5], Jiang et al. [23,21], Kuznetsov [29], Kuznetsov [30,31], Quintard et al. [40], Amiri and Vafai [4], Nield [37], Minkowycz et al. [34], Lee and Vafai [33], Mohamad [35], Rees and Pop [43], Jiang and Ren [20], Alazmi and Vafai [2], Baytas and Pop [8], Banu and Rees [6], Baytas [7], Saeid and Pop [45], Wong and Saeid [54]. Wang and Wang [53] also provide a perspective in their review article.

However, it appears that the *LTNE* model has only been utilized by Rees et al. [42], Wong et al. [55] and Saeid [44] for the application considered here — convection heat transfer from a horizontal circular cylinder. Rees et al. examined the problem of forced convection in the limit of high values of Péclet number. Their study was an analysis for the boundary layer regime by reducing the governing equations to a parabolic system. Later, this study was supplemented by Wong et al. who investigated the same problem but at finite Péclet number by numerically solving the fully elliptic governing equations. Saeid employed the thermal non-equilibrium condition to study free convection from a horizontal cylinder submerged in a porous medium but under the boundary-layer approximation. All

of these investigations ignored non-Darcian effects using the simple Darcy model, which is only valid for small Reynolds numbers (O(1) or less, based on the pore scale). Also, they neglected the effect of thermal dispersion, which can have a significant influence on heat transfer in porous systems, as explained in the literature.

As indicated above, heat transfer from cylinders immersed in a fluid-saturated porous media has practical importance in many engineering applications such as compact heat exchangers, nuclear reactors and solar power collectors. Therefore, in this paper, a more general flow model that incorporates non-Darcian effects, i.e., including the effects of solid boundaries, inertia and thermal dispersion, is combined with the *LTNE* model, to accurately predict forced convection heat transfer from a circular cylinder embedded horizontally in a porous medium consisting of a packed bed of spherical particles. The main objective of the present study is to analyze and quantify the effects of the particle diameter used for the porous bed on the heat transfer from an immersed cylinder without the assumption of thermal equilibrium between the phases. A deeper understanding of the effect of this parameter on both convective heat transfer and pressure drop in porous media systems may lead to improved optimization of heat exchangers for certain applications.

2. Analysis

The problem under consideration is forced convective flow over a circular cylinder immersed in a horizontal packed bed of spherical particles, as illustrated in Fig. 1. The fluid flow is assumed to be laminar and incompressible. The cylinder is isothermally heated at a constant temperature T_h and cooled by the incoming external flow at T_o. The confining horizontal walls have the same temperature T_w as the flow at the inlet. The blockage ratio of the bed is $D_{cy}/H = 0.25$, where D_{cy} is the cylinder diameter, which is considered the unit scale length, and H is the bed height. In analyzing the problem, the following assumptions are invoked: the porous medium is homogenous and isotropic, no heat generation occurs inside the porous medium, the inter-particle radiation heat transfer is ignored, the blockage ratio of the bed is small enough to neglect the channeling effect at the channel walls on the heat transfer from the cylinder surface. Importantly, local thermal equilibrium between the two phases is not assumed.

Based on these assumptions, the system of governing 2D equations of the average-volume continuity, Darcy–Brinkman–Forchheimer (*DBF*) momentum, and *LTNE* energy can be presented in the following vectorial form [38,27]:

$$\nabla\cdot\langle\acute{\mathbf{u}}\rangle = 0, \tag{1}$$

$$\frac{\rho_f}{\varepsilon}\left[\frac{\partial\langle\acute{\mathbf{u}}\rangle}{\partial\acute{t}}+\frac{1}{\varepsilon}\langle(\acute{\mathbf{u}}\cdot\nabla)\acute{\mathbf{u}}\rangle\right] = -\frac{\mu_f}{K}\langle\acute{\mathbf{u}}\rangle-\frac{\rho_f F\varepsilon}{\sqrt{K}}|\langle\acute{\mathbf{u}}\rangle|\langle\acute{\mathbf{u}}\rangle+\frac{\mu_f}{\varepsilon}\nabla^2\langle\acute{\mathbf{u}}\rangle-\nabla\langle\acute{P}_f\rangle, \tag{2}$$

$$\varepsilon(\rho c_p)_f\left[\frac{\partial\langle\acute{T}_f\rangle}{\partial\acute{t}}+\langle\acute{\mathbf{u}}\rangle\cdot\nabla\langle\acute{T}_f\rangle\right] = \nabla\cdot[k_{f.\mathrm{eff}}\nabla\langle\acute{T}_f\rangle]+h_{sf}a_{sf}(\langle\acute{T}_s\rangle-\langle\acute{T}_f\rangle), \tag{3}$$

$$(1-\varepsilon)(\rho c_p)_s\frac{\partial\langle\acute{T}_s\rangle}{\partial\acute{t}} = \nabla\cdot[k_{s.\mathrm{eff}}\nabla\langle\acute{T}_s\rangle]-h_{sf}a_{sf}(\langle\acute{T}_s\rangle-\langle\acute{T}_f\rangle). \tag{4}$$

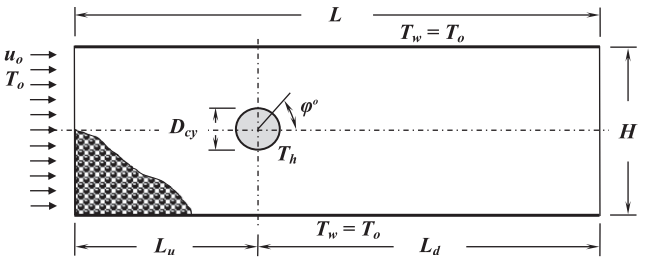

Fig. 1. Schematic diagram of the physical domain.

The *LTE* model uses the same momentum equations but replaces the thermal equations with the single energy

$$(\rho c_p)_m\frac{\partial\langle\acute{T}\rangle}{\partial\acute{t}}+\varepsilon(\rho c_p)_f[\langle\acute{\mathbf{u}}\rangle\cdot\nabla\langle\acute{T}\rangle] = \nabla\cdot[k_{f.\mathrm{eff}}\nabla\langle\acute{T}\rangle]. \tag{5}$$

Here $|\langle\acute{\mathbf{u}}\rangle| = \sqrt{\acute{u}^2+\acute{v}^2}$ and $(\rho c_p)_m = \varepsilon(\rho c_p)_f + (1-\varepsilon)(\rho c_p)_s$. The operator $\langle\cdots\rangle$ denotes a local volume average of a quantity. Eqs. (1)–(5) are transformed into a non-dimensional form (7)–(11) employing the following dimensionless variables

$$x,y = \frac{\acute{x},\acute{y}}{D_{cy}},\quad \mathbf{u} = \frac{\acute{\mathbf{u}}}{u_o},\quad t = \frac{\acute{t}u_o}{D_{cy}},\quad \theta = \frac{\acute{T}-T_o}{(T_h-T_o)},\quad P_f = \frac{\acute{P}_f}{\rho_f u_o^2}, \tag{6}$$

$$\nabla\cdot\langle\mathbf{u}\rangle = 0, \tag{7}$$

$$\frac{\partial\langle\mathbf{u}\rangle}{\partial t}+\frac{1}{\varepsilon}\langle(\mathbf{u}\cdot\nabla)\mathbf{u}\rangle = -\frac{\varepsilon}{Re_D.Da}\langle\mathbf{u}\rangle-\frac{F\varepsilon^2}{\sqrt{Da}}|\langle\mathbf{u}\rangle|\langle\mathbf{u}\rangle+\frac{1}{Re_D}\nabla^2\langle\mathbf{u}\rangle-\varepsilon\nabla\langle P_f\rangle, \tag{8}$$

$$\frac{\partial\langle\theta_f\rangle}{\partial t}+\langle\mathbf{u}\rangle\cdot\nabla\langle\theta_f\rangle = \frac{1}{\varepsilon Re_D Pr}\left[\frac{\partial}{\partial x}\left(\frac{k_{f.\mathrm{eff},x}}{k_f}\frac{\partial\langle\theta_f\rangle}{\partial x}\right)+\frac{\partial}{\partial y}\left(\frac{k_{f.\mathrm{eff},y}}{k_f}\frac{\partial\langle\theta_f\rangle}{\partial y}\right)\right] + \frac{Bi.k_r}{\varepsilon Re_D Pr}(\langle\theta_s\rangle-\langle\theta_f\rangle), \tag{9}$$

$$\frac{\partial\langle\theta_s\rangle}{\partial t} = \frac{\alpha_r}{(1-\varepsilon)Re_D Pr}\nabla\cdot\left[\frac{k_{s.\mathrm{eff}}}{k_s}\nabla\langle\theta_s\rangle\right]-\frac{Bi.\alpha_r}{(1-\varepsilon)Re_D Pr}(\langle\theta_s\rangle-\langle\theta_f\rangle) \tag{10}$$

and the dimensionless form of the *LTE* energy model becomes

$$\frac{\partial\langle\theta\rangle}{\partial t}+(\varepsilon/C)[\langle\mathbf{u}\rangle\cdot\nabla\langle\theta\rangle] = \frac{1}{Re_D Pr.C}\nabla\cdot\left[\frac{k_{f.\mathrm{eff}}}{k_f}\nabla\langle\theta\rangle\right], \tag{11}$$

where, $C = \varepsilon + (1-\varepsilon)(k_r/\alpha_r)$, and k_r and α_r are the solid/fluid thermal conductivity and diffusivity ratios, k_s/k_f and α_s/α_f, respectively. In addition, the Reynolds, Darcy, Prandtl, and Biot numbers are defined, respectively, as:

$$Re_D = \frac{u_o D_{cy}\rho_f}{\mu_f},\quad Da = \frac{K}{D_{cy}^2},\quad Pr = \frac{\nu_f}{\alpha_f},\quad Bi = \frac{D_{cy}^2 h_{sf}a_{sf}}{k_s}, \tag{12}$$

where a_{sf} is the specific surface area of the packed bed that can be expressed as suggested by Dullien [14]:

$$a_{sf} = \frac{6(1-\varepsilon)}{d_p}. \tag{13}$$

The formulation of the interfacial heat transfer coefficient h_{sf} in the present investigation is based on the empirical correlation proposed by Wakao et al. [51] for packed beds and can be expressed as:

$$h_{sf} = \frac{k_f}{d_p}\left[2+Pr^{1/3}\left(\frac{\rho_f|\mathbf{u}|d_p}{\mu_f}\right)^{0.6}\right]. \tag{14}$$

In turn, this allows the Biot number to be expressed as:

$$Bi = 6(1-\varepsilon)\left(\frac{1}{k_r}\right)\left(\frac{D_{cy}}{d_p}\right)^2\left[2+Pr^{1/3}\left(\frac{\rho_f|\mathbf{u}|d_p}{\mu_f}\right)^{0.6}\right], \tag{15}$$

which explicitly shows the strong effect of the interfacial heat transfer rate on the particle to cylinder diameter.

The permeability of the porous medium K and the geometric function F in the momentum equation are inherently tied to the structure of the porous medium. These are generally based on empirical fits from experimental findings, i.e., no universal representations exist. For a randomly packed bed of spheres such coefficients were reported by Ergun [15] and were expressed in terms of porosity ε and particle diameter d_p as follows:

$$K = \frac{\varepsilon^3 d_p^2}{150(1-\varepsilon)^2}, \quad F = \frac{1.75}{\sqrt{150\varepsilon^3}}. \tag{16}$$

The effective thermal conductivity of the fluid phase $k_{f.\text{eff}}$ is composed of a sum of the stagnant k_{st} and dispersion k_d conductivities: $k_{f.\text{eff},\,(x,\,y)} = k_{st} + k_{d(x,\,y)}$. In this study the stagnant conductivity depends on the conductivities of the fluid and the solid phases, and is obtained from the semi-theoretical model of Zehner and Schluender [56]:

$$\frac{k_{st}}{k_f} = (1-\sqrt{1-\varepsilon}) + \frac{2\sqrt{1-\varepsilon}}{1-\lambda B}\left[\frac{(1-\lambda)B}{(1-\lambda B)^2}\ln(\lambda B) - \frac{B+1}{2} - \frac{B-1}{1-\lambda B}\right], \tag{17}$$

where $\lambda = 1/k_r$ and $B = 1.25[(1-\varepsilon)/\varepsilon]^{\frac{10}{9}}$. Whereas, the dispersion conductivity that incorporates the additional thermal transport due to the fluid's tortuous path around the solid particles is determined in both longitudinal and lateral directions based on the experimental correlation reported by Wakao and Kaguei [50], and is given by:

$$\frac{k_{dx}}{k_f} = 0.5Pr\left(\frac{\rho_f|\mathbf{u}|d_p}{\mu_f}\right), \quad \frac{k_{dy}}{k_f} = 0.1Pr\left(\frac{\rho_f|\mathbf{u}|d_p}{\mu_f}\right). \tag{18}$$

The solid effective thermal conductivity has a stagnant component only since it is stationary:

$$k_{s.\text{eff}} = (1-\varepsilon)k_s. \tag{19}$$

Dirichlet boundary conditions, for the pertinent variables, i.e., the velocity and temperature, are imposed on the inlet and solid boundaries, while Neumann boundary conditions are imposed at the outlet. Thus, the non-dimensional initial and boundary conditions can be expressed mathematically as:

$$\begin{aligned}
&\text{at } t = 0: \ u = v = \theta_f = \theta_s = 0,\\
&\text{at } t > 0: \ u = u_o, \quad v = \theta_f = \theta_s = 0 \quad \text{at } (x = 0,\ 0 < y < H),\\
&\frac{\partial u}{\partial x} = \frac{\partial \theta_f}{\partial x} = \frac{\partial \theta_s}{\partial x} = v = 0 \quad \text{at } (x = L,\ 0 < y < H),\\
&u = v = 0 = \theta_f = \theta_s = 0 \quad \text{at} \quad (0 < x < L,\ y = 0 \quad \text{and} \quad H),\\
&u = v = 0,\ \theta_f = \theta_s = 1 \text{ at cylinder boundary.}
\end{aligned} \tag{20}$$

It is assumed that the fluid and solid phases share the same temperature as the isothermal surface of the cylinder, i.e., thermal equilibrium is imposed at the heated boundary (e.g., [2] and [54]). Heat transfer characteristics are evaluated based on the time-mean average Nusselt numbers along the heated cylinder for the fluid and solid phase as follows:

$$\begin{aligned}
Nu_f &= \frac{h_{cy}D_{cy}}{k_f} = \frac{-k_{f.\text{eff}}\int_0^S[\partial \acute{T}_f/\partial n]dsD_{cy}}{k_f(T_h - T_o)},\\
Nu_s &= \frac{h_{cy}D_{cy}}{k_s} = \frac{-k_{s.\text{eff}}\int_0^S[\partial \acute{T}_s/\partial n]dsD_{cy}}{k_s(T_h - T_o)},
\end{aligned} \tag{21}$$

where n and s denote to the normal and tangential directions at the cylinder surface, respectively, and S is the periphery of the cylinder. Whereas, the pressure drop is calculated as:

$$\triangle P_f = |\rho_f u_o^2(P_{f.out} - P_{f.in})|, \tag{22}$$

where the subscripts *out* and *in* refer to the outlet and inlet of the channel.

3. Numerical method of solution

Eqs. (7)–(11) have been solved using a spectral-element method, which is essentially a high-order finite-element method, Karniadakis et al. [26] and Thompson et al. [47]. For spatial discretisation, this method employs tensor-product Lagrange polynomials, associated with Gauss–Legendre–Lobatto quadrature points, as shape functions over each quadrilateral element. In this way, the spatial resolution can be varied by either changing the number of quadrilateral elements (h refinement), or by changing the order of the Lagrange polynomial shape functions (p refinement). For the current study, a polynomial order of $p = 6$ was employed. In the current implementation, curvature of the element boundaries is accounted for, hence complex geometries can be accurately modeled.

For the temporal discretization, a two- and three-step time-splitting scheme, described in Karniadakis et al. [26] and Thompson et al. [47], is used for the energy and momentum equations. For the energy equations, this results in separate equations being formed for the nonlinear advection term and the linear diffusion term. For the momentum equations, a third equation is required for the pressure. A Poisson equation is formed for the pressure term by enforcing continuity at the end of the pressure substep. The nonlinear advection equation is solved using a third-order Adams–Bashforth method, and the linear diffusion equation is solved using a second-order Crank–Nicholson method. Importantly the Darcy term in the momentum equation is treated implicitly together with diffusion term in the linear sub-step. This reduces the otherwise severe timestep restriction that results if the Darcy term is treated explicitly. For the forced convection regime which is the case considered in this paper, where buoyancy effects can be neglected, the momentum and energy equations decouple.

3.1. Grid independency of the results

Tests were conducted to ensure that the numerical results obtained are independent of the spatial grid resolution. A grid resolution study (*GRS*) was undertaken for the configuration of the circular cylinder mounted between two parallel walls as shown in Fig. 1. To sufficiently resolve the higher temperature gradients near the heated cylinder the macro-element distribution was concentrated towards its surface. The macro-mesh resolution is decreased in both the upstream and downstream directions to the inlet and outlet boundaries where gradients are smaller. To capture the boundary layers in the y-direction a finer mesh is employed near the walls with coarsening towards the core of the channel. The typical computational macro-mesh for the physical domain is described in Fig. 2. The *GRS* was undertaken for $Re_D = 1$ and 250, and for two values of the particle size $D_{cy}/d_p = 10$ and 100. This was done by varying the polynomial order p within the range 2–8, while keeping the macro-element layout the same, in order to ascertain at what spectral resolution the solution becomes grid independent and subsequently which resolution provides a satisfactory compromise between accuracy and computational expense. An advantage of the spectral-element method is the ability to set p at run-time, allowing resolution studies to be performed more easily. Nu_f and Nu_s were monitored in this study as an indicator of convergence. The results in Table 1 showed that Nu_f and Nu_s are converged by $p = 6$ with a relative error of less than 0.5%.

3.2. Verification of the numerical algorithm

The implementation of the equations into the software was checked through comparisons of predictions against previously

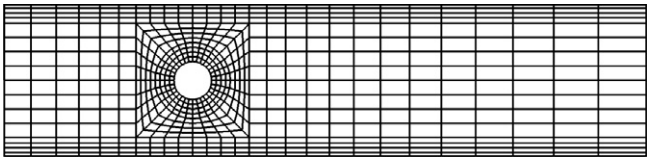

Fig. 2. Typical computational domain.

published numerical and experimental results. First, velocity and heat transfer data for a cooling air jet impinging on an isothermal heated surface immersed in a confined porous channel under the *LTNE* condition was calculated and compared to the numerical predictions for the identical problem presented in Wong and Saeid [54]. For this data, the interfacial convective heat transfer coefficient is $H_v = 1.0$, the porosity-scaled fluid/solid thermal conductivity ratio is $K_r = 1.0$, the Darcy number is $Da = 10^{-3}$, and the porosity is $\varepsilon = 0.87$. Fig. 3(a) presents the velocity distribution close to the wall being impinged upon, and Fig. 3(b) presents the variation of Nusselt number Nu of the fluid and solid phase from the heat source against Pe′clet number Pe. As shown in these figures, there are small differences in the results between the two numerical models. The differences may be a result of the lower-order numerical model used by Wong and Saeid. They used a finite-volume model with a lower-order power-law scheme for the convection–diffusion formulation to discretise their governing equations. Also, they did not state the values of the thermal diffusivity and heat capacity of the alloy of metal foam used as their porous medium. These values had to be estimated from data for the original alloy components [Fe(73%)Cr(20%)Al(5%)Y(2%)] based on their percentages. The different comparisons clearly show very similar trends. For the Nusselt number variations shown in Fig. 4, the current prediction is approximately 10% lower for the fluid medium than the prediction of Wong and Saied, and considerably better for the solid medium.

Second, the numerical results were benchmarked against experimental results obtained by Nasr et al. [36] for the air forced convection heat transfer around a circular cylinder embedded in a packed bed of spherical particles. The comparison is presented in Fig. 4. Two kinds of particle materials, nylon and aluminum, were chosen as the solid phase with solid/fluid thermal conductivity ratios $k_r = 8.7$ and 7605, and with different sizes, $d_p = 6.35$ and 12.23 mm, respectively. As recommended in their paper, the model of Zehner and Schluender [56] was used to calculate the effective stagnant thermal conductivity in the energy equation while the dispersion-enhanced conductivity was neglected. The porous medium was treated as a continuum by volume-averaging the thermal diffusivity of the solid and fluid phases. There is clearly good agreement between the numerical predictions, the experimental results and, as a further comparison, with the analytical solutions made by Cheng [11] for mixed convection about a horizontal cylinder embedded in a fluid-saturated porous medium. Cheng obtained similarity solutions using the Darcy model in the boundary-layer region.

4. Results and discussion

The results focus on the effect of the particle diameter d_p of a packed bed of spherical particles on the heat transfer and thermal characteristics around an embedded circular cylinder, and the pressure drop through the bed. The numerical calculations have been carried out for the following ranges of the parameters: $D_{cy}/d_p = 100$–10, $Re_D = 1$–250 and $k_r = 0.01$–1000, with the Darcy number determined by Eqs. (12) and (16) and varying within the range of $Da = 3.333 \times 10^{-7} - 3.333 \times 10^{-5}$, and with the porosity set to $\varepsilon = 0.5$. The thermal and flow states are independent of α_r because only time-steady cases are considered in this paper. These parameter ranges were chosen based both on previous studies published in the literature and to include typical combinations for physical systems. For instance, with water as the working fluid with $k_f = 0.609$ W/m K and $Pr = 7.0$, k_r can vary significantly. For example, if the porous medium consists of Silicon Carbide (SiC) with $k_s = 420$ W/m K, $k_r \simeq 700$, towards the upper end of our chosen range, while Balsa wood has $k_s = 0.055$ W/m K, giving $k_r \simeq 0.1$, which is towards the lower end. The results presented have been obtained using the *LTNE* model; however, the last subsection of this section presents a comparison between the equilibrium (*LTE*) and non-equilibrium (*LTNE*) energy models.

4.1. Effect of particle diameter

As described previously there are some conflicting conclusions concerning the dependency of the convective heat transfer on d_p. Therefore this section focusses on this dependency as Re_D and k_r are varied. Fig. 5 shows the variation of the time-mean average fluid Nusselt number Nu_f against D_{cy}/d_p for the entire range of $Re_D = 1$–250, at $k_r = 1.0$. Clearly, Nu_f decreases or increases as d_p increases, depending firstly on Re_D, and then on the particular range of D_{cy}/d_p considered. For example, at $Re_D = 1$ and 10, Nu_f decreases with increasing d_p; however, for $Re_D > 40$, a consistent increase in Nu_f can be seen as d_p increases, whereas, at $Re_D = 40$, Nu_f decreases for the range of $D_{cy}/d_p = 100$–50, but above this range, Nu_f begins to increase considerably. The empirical expressions for the permeability K and thermal dispersion k_d, given in Eqs. (16) and (18), respectively, show that these two parameters increase as d_p increases. The convection heat transfer should be intensified by increasing k_d, whereas an increase in K weakens the mixing of the fluid by the porous medium and consequently reduces the convective heat transfer. At low values of $Re_D < 40$, the influence of k_d, which is a direct function of the Reynolds number based on the pore scale Re_p, is much less than and dominated strongly by that of K, and of the stagnant thermal conductivity k_{st} which is in turn a function of k_r. Therefore, the additional thermal dispersive conductivity resulting from the increase in d_p is not great enough to increase k_d significantly. Thus, the consequent convective heat transfer enhancement may not be enough to counterbalance the decrease in the convection heat transfer resulting from the change to K and k_{st}. However, at moderate and high values of $Re_D > 40$, the effect of k_d becomes stronger relative to K and k_{st}, and the heat transfer then increases as d_p increases. Indeed, the interesting decrease-increase trend of Nu_f with D_{cy}/d_p shown in Fig. 5 at

Table 1
Grid resolution study of the computational domain for two values of the particle diameter $D_{cy}/d_p = 10$ and 100, and at $Re_D = 1.0$ and 250.

p	$Re_D = 1.0$				$Re_D = 250$			
	$D_{cy}/d_p = 10$		$D_{cy}/d_p = 100$		$D_{cy}/d_p = 10$		$D_{cy}/d_p = 100$	
	Nu_f	Nu_s	Nu_f	Nu_s	Nu_f	Nu_s	Nu_f	Nu_s
2	2.40902	0.18507	2.59665	0.19379	91.56000	0.27368	40.92436	0.34906
3	2.40426	0.18471	2.58346	0.19372	91.37153	0.27304	40.55497	0.34740
4	2.40099	0.18439	2.57862	0.19361	91.35897	0.27273	40.61156	0.34700
5	2.39874	0.18418	2.57519	0.19346	91.31966	0.27252	40.76205	0.34678
6	2.39718	0.18404	2.57388	0.19336	91.29128	0.27238	40.80610	0.34662
7	2.39606	0.18393	2.57318	0.19328	91.27201	0.27228	40.81810	0.34651
8	2.39521	0.18385	2.57261	0.19321	91.25765	0.27220	40.82188	0.34644

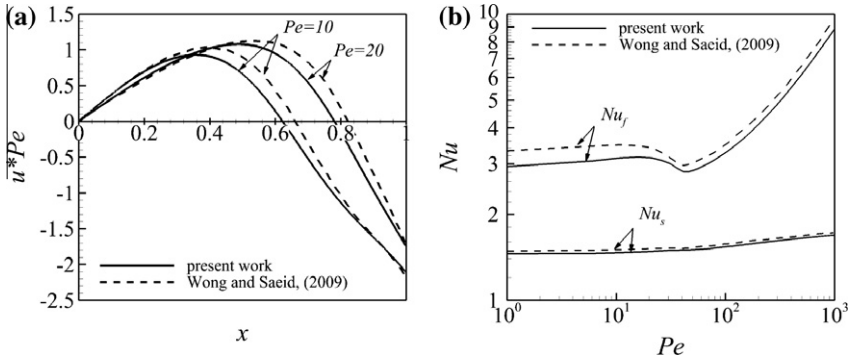

Fig. 3. Comparison between two numerical models: the present model and the model used by Wong and Saied 54, (a) for the variation of (u-velocity $\times$ Pe) at y = 0.002 along the heat source, for two values of Pe = 10 and 20, (b) for the variation of Nusselt number Nu of the fluid and solid phase against Pe.

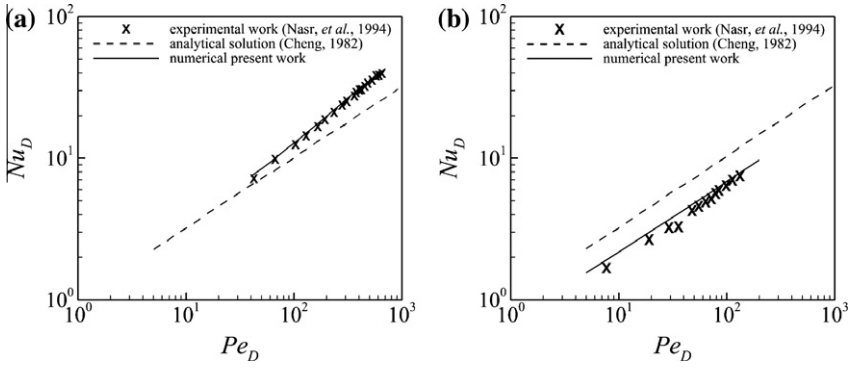

Fig. 4. Comparison between the present algorithm with the experimental work done by Nasr et al. [36], for air forced convection heat transfer around a circular cylinder, D = 12.7 mm, embedded in a, (a) packed bed of nylon spheres, d_p = 6.35 mm, and (b) packed bed of aluminum spheres, d_p = 12.23 mm, with porosity ε = 0.37 for both the beds.

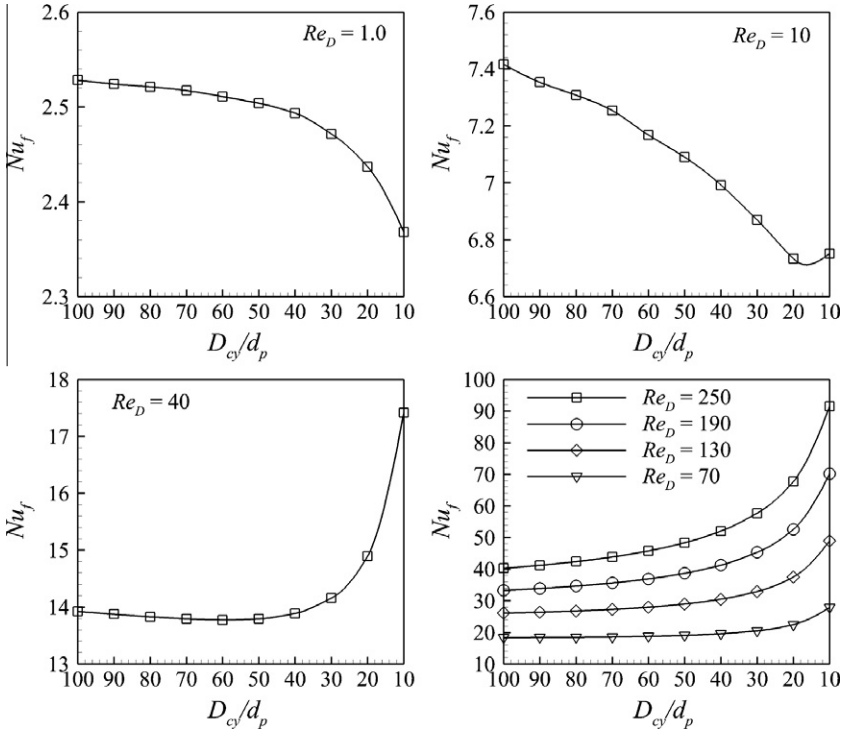

Fig. 5. The variation of time-mean average fluid Nusselt number Nu_f versus cylinder-to-particle diameter ratio D_{cy}/d_p at Re_D ranging from 1 to 250, for a heated circular cylinder embedded in a horizontal packed bed of spheres using the *LTNE* energy model, and at k_r = 1.0.

$Re_D = 40$ gives a clear depiction of competition between the different physical effects on heat transfer.

Fig. 6 displays the variation of the time-mean average solid Nusselt number Nu_s with D_{cy}/d_p at different Re_D, for $k_r = 1.0$. It can be seen that Nu_s decreases with increasing d_p due to the decrease in the contact surface area (*CSA*) between the particles and the heated surface of the cylinder. There is a clear influence from Re_D on this variation, whereas the change in Nu_f with D_{cy}/d_p becomes significant at higher Re_D. The figure shows that the influence of Re_D diminishes at larger particle size. However, the overall change in Nu_s at any d_p is only a factor of 2 as the Reynolds number is varied by a factor of 25. In addition, the effect of d_p on the fluid and solid temperature fields around the cylinder is shown in Fig. 7 at $Re_D = 10$ and 250, for $k_r = 1.0$. Interestingly, it is found that an increase in d_p acts to enlarge the fluid thermal boundary layer (*FTBL*). This means that the increase of Nu_f with D_{cy}/d_p for $Re_D > 40$, shown in Fig. 5, does not result from the direct impact of the normal temperature gradient at the cylinder's surface, but instead mainly from the effect of k_d. The isotherms of the two phases seem to be identical which indicates to the thermal equilibrium state in the bed. This is due to the fact that at $k_r = 1.0$, the calculated value of *Bi* using Eqs. (12)–(15) is large enough to create a strong thermal convective contribution between both phases and leads to the equilibrium state. According to these equations, increasing the value of k_r decreases *Bi*, and may lead to significantly different thermal fields for the fluid and solid phases. Fig. 8 shows the thermal fields for both phases at $k_r = 1000$. Even at this high k_r, *Bi* is still large enough to generate almost similar thermal fields for the phases. But, it is obvious that the difference between the two fields increases as Re_D and/or d_p increases.

Some researchers, for instance, Jiang et al. [23,21,25], have suggested that the conflicting results concerning the effect of d_p on Nu_f may result from the difference in the solid and fluid thermal conductivities, i.e., k_r. They mentioned that when these conductivities are of the same order, an increase in Nu_f can be obtained as d_p increases, as in, for example, Kwendakwema and Boehm [32], Wang and Du [52], and David and Cheng [13]. However, when the solid thermal conductivity is much larger than that of the fluid, Nu_f decreases as d_p increases, such as in the results of Jeigarnik et al. [19], Nasr et al. [36], and Saito and Lemos [46]. To investigate this further, Fig. 9 presents the effect of k_r on the dependency of Nu_f on d_p, at different Re_D. First, it is obvious that the effect of k_r becomes significant only at low Re_D, i.e., $Re_D < 40$. At $Re_D = 40$ for the range of $D_{cy}/d_p = 100$–50, the trend of Nu_f changes from positive to negative by increasing k_r from 0.01 or 1.0 to 1000. Otherwise, this effect diminishes due to the dominance of k_d on k_{st}. Second, at this low range of Re_D, which allows the effect of k_r to emerge, unexpectedly it is found that Nu_f decreases as d_p increases when $k_r \leqslant 1$, while it increases with increasing *dp* at $k_r = 1000$.

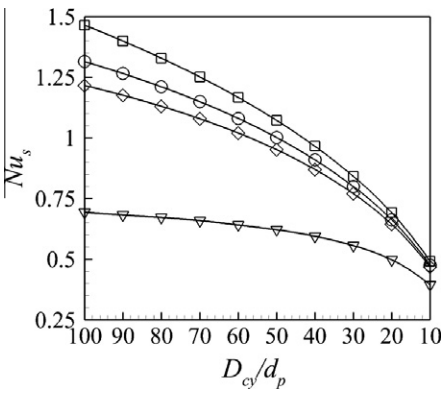

Fig. 6. The variation of time-mean average solid Nusselt number Nu_s with cylinder-to-particle diameter ratio D_{cy}/d_p for different Re_D; (▽) 10, (◇) 40, (○) 100 and (□) 250, and at $k_r = 1.0$.

The physical explanation for the behavior of the current results presented in Fig. 9 is that the fluid region around the heated cylinder is seen to be mainly controlled by diffusion heat transfer at low Re_D. Therefore, for $k_r \leqslant 1$, most of the heat transferred from the heated surface releases throughout the fluid phase by conduction. Also, the inter-phase convective heat transfer, which is often referred to in the literature as the *"fin effect"*, is acting from the fluid to the solid phase due to the poor conduction in the solid phase at low k_s. In spite of the fact that the increase in d_p increases the *"fin effect"* owing to the increase in the interfacial surface area, (which leads to an increase in Nu_f), it also increases the amount of conductive heat transferring within the fluid phase due to the decrease in the *CSA* between the solid particles and the cylinder surface as previously mentioned. The effect of the *CSA* seems to be higher than that of the *"fin effect"*, consequently, a slight decrease in Nu_f is obtained with increasing d_p. It is also shown that the influence of the *CSA* becomes significant at large d_p. However, by increasing k_r to 1000, the conduction heat transfer to the solid particles becomes strong enough to balance that to the fluid phase particularly at small d_p; therefore, the interfacial *"fin effect"* is expected to be almost negligible. However, as d_p increases, the solid conductive heat transfer decreases and the *"fin effect"* from the fluid to the solid increases, and then Nu_f increases.

The effect of k_r on how Nu_f varies with d_p, shown in Fig. 9, has an opposite trend to some previously published findings. The comparison in the next sub-section between the predictions from the *LTNE* and *LTE* energy models helps to address this discrepancy.

4.2. Comparison between the LTNE and LTE models

A comparison between the *LTNE* and *LTE* energy models on the variation of Nu_f with D_{cy}/d_p as Re_D and k_r are varied, is given in Figs. 10–12. These figures are presented for $k_r = 0.01$, 1.0 and 1000, respectively, and at $Re_D = 1.0$, 10, 40 and 250. The first two Figs. 10 and 11, for $k_r = 0.01$ and 1.0, respectively, show that the *LTE* model predicts exactly the same general trend for the variation of Nu_f as the *LTNE* model, and at all values of Re_D. In addition, there is less than a 10% difference in the values of the Nusselt number for the entire Reynolds number range covered. However, interestingly, Fig. 12 for $k_r = 1000$, shows that both energy models produce different trend of results, but only at the same low range of Re_D mentioned prior, i.e., $Re_D < 40$ and for $D_{cy}/d_p = 100$–50 at $Re_D = 40$, due to the weakness in the effect of thermal dispersion k_d at this range of Re_D. Thus, it is clearly seen that the increasing trend of Nu_f as d_p increases at high $k_r = 1000$ using the *LTNE* model is reversed for the *LTE* model, i.e., Nu_f decreases as d_p increases. Apart from the differences in trends, the higher k_r does result in a substantial change to the predicted Nusselt numbers for the two cases. For example, for $Re_D = 40$, there is a difference between the Nusselt numbers by a factor of six for large D_{cy}/d_p. This difference is less for larger particles but still substantial.

In addition, the figures show that the fluid Nusselt number for the two-phase porous system evaluated using the *LTNE* model approaches that for the *LTE* model when the interfacial heat transfer coefficient approaches zero, i.e., $h_{sf} \to 0$. Eq. (15) shows that this coefficient is proportional to k_f and inversely proportional to d_p, with a weaker dependence on the Prandtl number and local Reynolds number. Indeed, Fig. 12 at constant $k_r = 1000$ reveals that the discrepancy between the two models decreases as d_p increases and/or Re_D decreases. In non-dimensional terms, the equivalent situation occurs for $Bi \to 0$ in Eq. 12, leading the inter-phase convective term in the *LTNE* model to vanish. For *steady-state* solutions, the

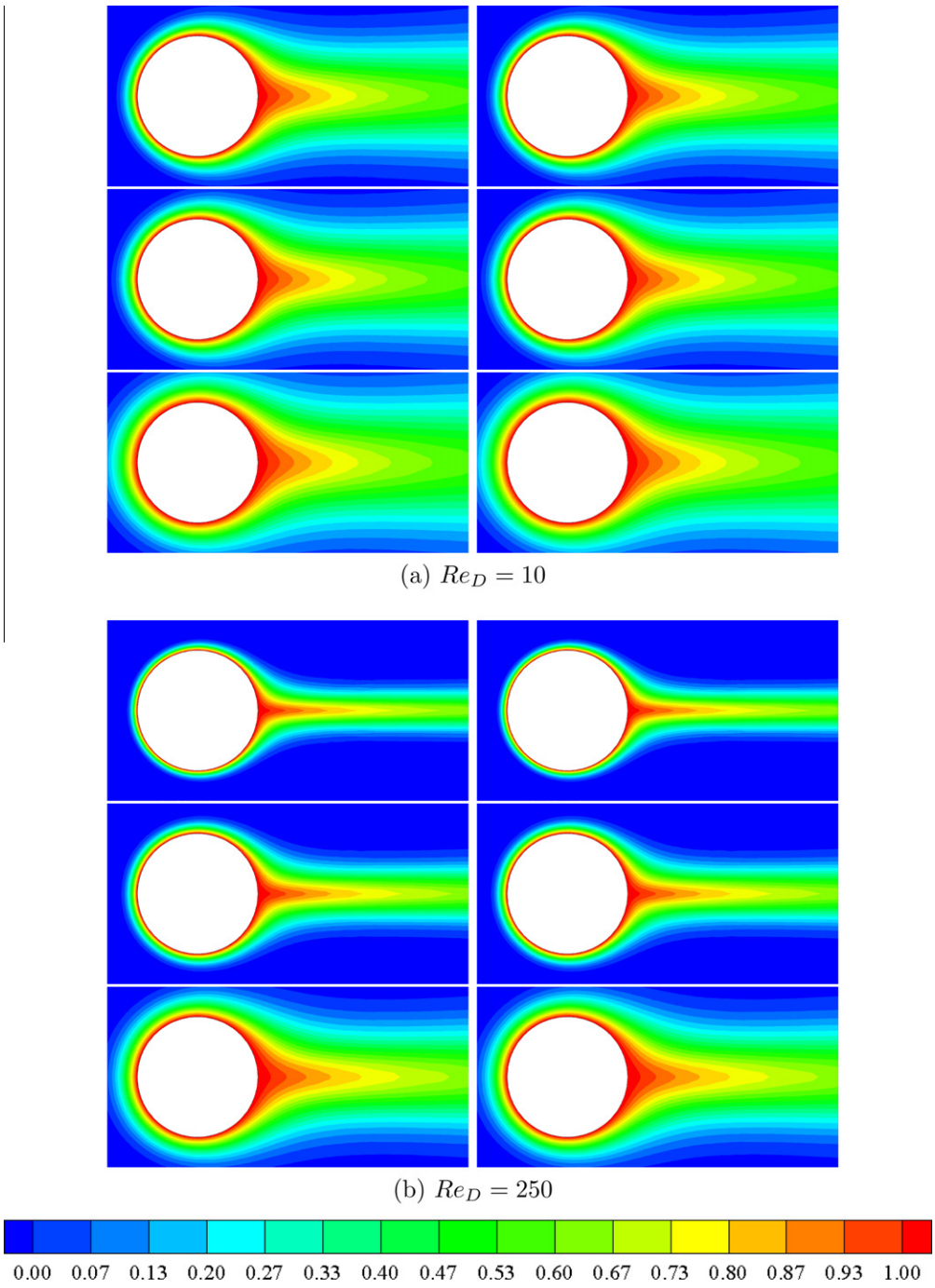

Fig. 7. Fluid (left) and solid (right) isotherms, around a heated circular cylinder embedded in a horizontal packed bed of spheres at; (a) $Re_D = 10$, and (b) $Re_D = 250$, for three values of D_{cy}/d_p, from top to bottom 100, 40 and 10. The isotherms are for $k_r = 1.0$.

LTNE equation for the fluid temperature reduces to that for the *LTE* model, despite the fact that thermal equilibrium does not apply.

If $h_{sf} \to 0$ physically this means that the solid phase is effectively insulated from the fluid, and therefore the convective interaction between them by the *"fin effect"* is suppressed. This interaction is the most important factor required to obtain the same thermal fields for both phases, and leads to a thermal equilibrium state. Moreover, at this case, the influence of the contact surface area *CSA* still remains, which increases the fluid conductive heat transfer as d_p increases, and consequently decreases Nu_f. Therefore, it can be concluded that the essential reason for obtaining a decrease in Nu_f with increasing d_p at high k_r and low Re_D, as in Nasr et al. [36], Jeigarnik et al. [19] and Saito and Lemos [46], is either from using the *LTE* model, or from circumstances that lead to a low interfacial convective heat transfer coefficient h_{sf} in the *LTNE* model or their experiments. Note that the current results do not show any increase in Nu_f as d_p increases when $k_r \leqslant 1.0$ for low Re_D.

Furthermore, the figures also display that the values of Nu_f predicted by the *LTE* model are always higher than those predicted by the *LTNE* model for $k_r \geqslant 1.0$. This is presumably due to the continuum assumption in the *LTE* model to calculate the thermal properties, i.e., k_r and α_r, of the porous medium. Also, as mentioned above

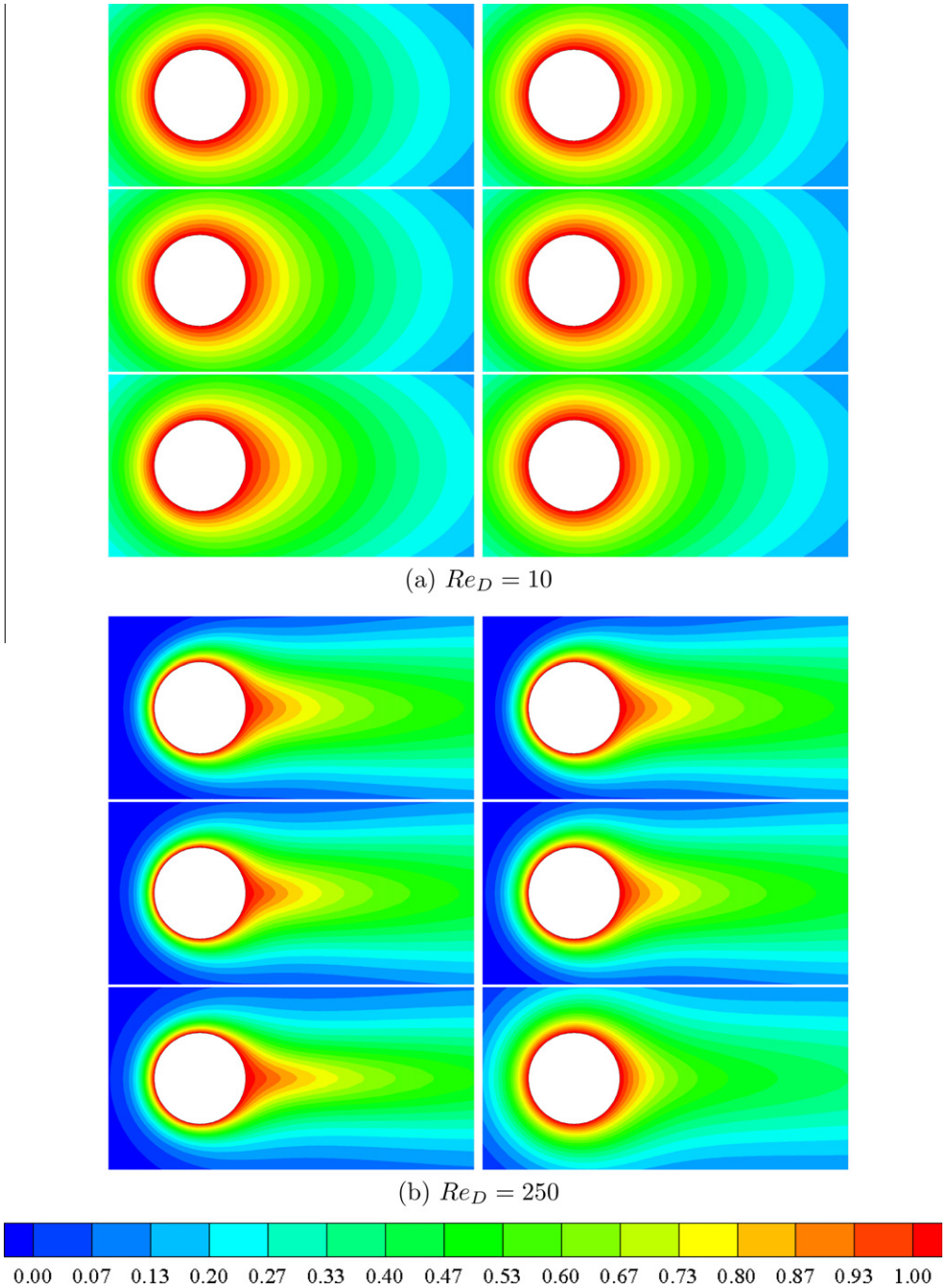

Fig. 8. Fluid (left) and solid (right) isotherms, around a heated circular cylinder embedded in a horizontal packed bed of spheres at; (a) $Re_D = 10$, and (b) $Re_D = 250$, for three values of D_{cy}/d_p, from top to bottom 100, 40 and 10. The isotherms are for $k_r = 1000$.

the difference between the two models increases as d_p decreases or as Re_D increases. It is also obviously clear that this difference increases as k_r or h_{sf} increases.

4.3. Pressure drop and heat transfer enhancement

It is well known from the literature that the presence of porous media always increases the pressure drop, which may be unfavorable in many thermal applications, for example, in heat exchangers, since bigger pumps will be required. Therefore, both pressure drop and heat transfer augmentation influences of porous media must be taken into consideration in the design of heat exchangers. Fig. 13 shows the pressure drop (ΔP_f) in the porous channel compared with an empty channel, and the percentage of the heat transfer enhancement (% *HTE*) resulting from packing the empty channel by spherical porous materials, as a function of Re_D for different D_{cy}/d_p. The results presented in this figure are predicted at $k_r = 1.0$, and the %*HTE* is calculated as follows:

$$\%HTE = \frac{Nu_{t.porous} - Nu_{empty}}{Nu_{empty}} \times 100\% \tag{23}$$

Generally, it can be seen that although the use of porous materials can be an excellent method for *HTE*, it may lead to a several orders-of-magnitude increase in pressure drop. However, the plots in Fig. 13(a) show that this high ΔP_f decreases dramatically with increasing d_p. Larger particle diameters decrease the contact area

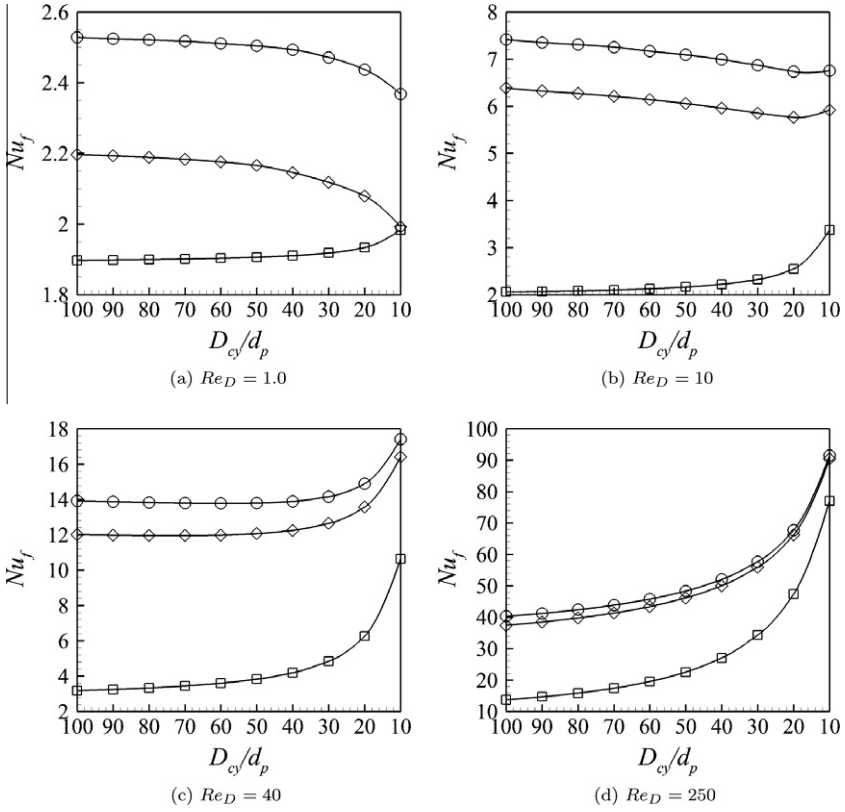

Fig. 9. The effect of solid-to-fluid thermal conductivity ratio k_r: (◇) 0.01, (○) 1.0, and (□) 1000, on the variation of Nu_f versus D_{cy}/d_p, at Re_D: (a) 1.0, (b) 10, (c) 40, and (d) 250.

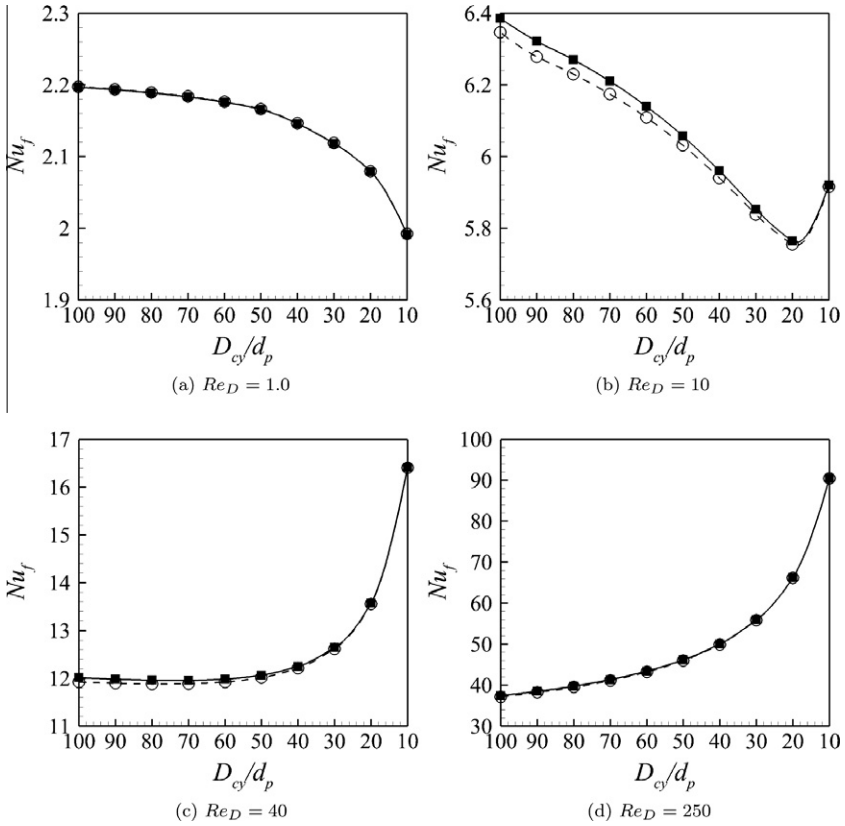

Fig. 10. Comparison between the *LTNE* (*solid line with* ■) and the *LTE* (*dash line with* ○) energy models for the variation of Nu_f versus D_{cy}/d_p for Re_D; (a) 1.0, (b) 10, (c) 40, and (d) 250. The results are obtained at $k_r = 0.01$.

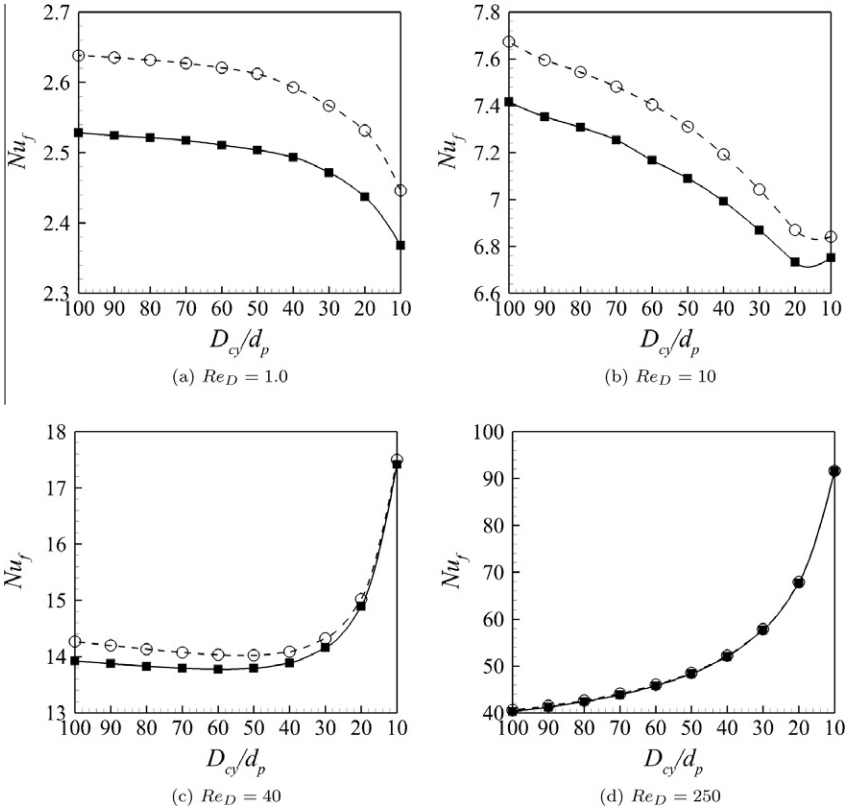

Fig. 11. Comparison between the *LTNE* (*solid line with* ■) and the *LTE* (*dash line with* ○) energy models for the variation of Nu_f versus D_{cy}/d_p for Re_D; (a) 1.0, (b) 10, (c) 40, and (d) 250. The results are obtained at $k_r = 1.0$.

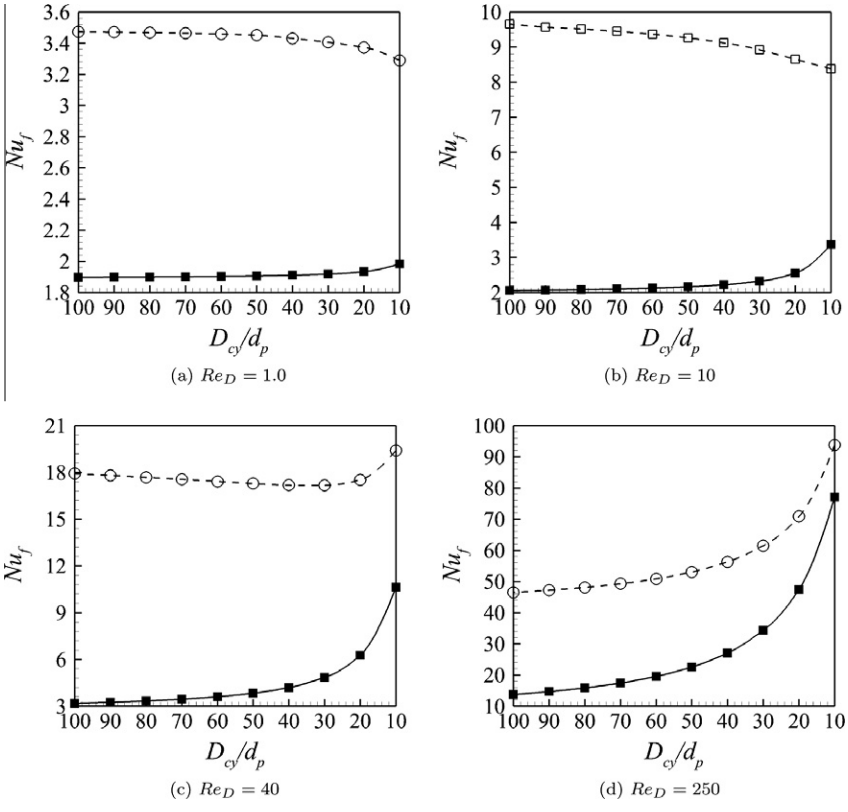

Fig. 12. Comparison between the *LTNE* (*solid line with* ■) and the *LTE* (*dash line with* ○) energy models for the variation of Nu_f versus D_{cy}/d_p for Re_D; (a) 1.0, (b) 10, (c) 40, and (d) 250. The results are obtained at $k_r = 1000$.

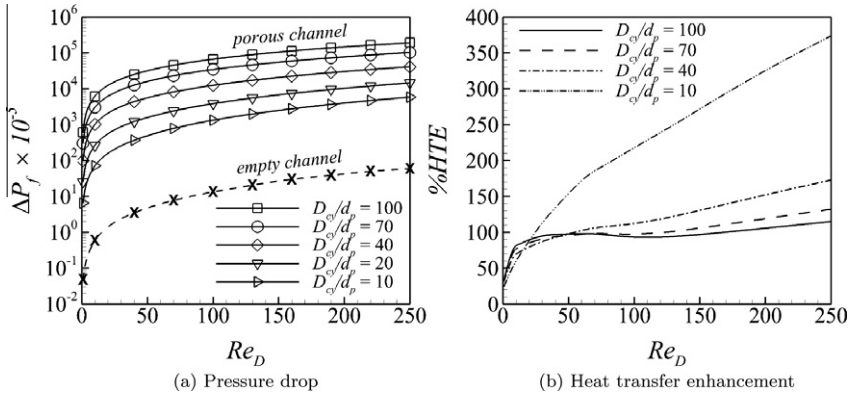

Fig. 13. The effect of the particle diameter d_p of a packed bed of spheres on; (a) the pressure drop during the bed, compared with that for an empty channel, and (b) the percentage of the heat transfer enhancement *%HTE*, for a range of Re_D = 1–250, and at k_r = 1.0.

between the particles and increase the pore size and thus the permeability of the packed bed, which leads to a decrease in the flow resistance or ΔP_f. The plots in Fig. 13(b) show that a sizeable *%HTE* can be obtained at large d_p and high Re_D. Therefore, it can be concluded that a reasonable increase in *HTE* with a significant relative decrease in ΔP_f, which is the optimal case for any thermal application using porous media as an enhancement mechanism for heat transfer, can be achieved with high values of d_p.

5. Concluding remarks

In the present paper, the effect of particle diameter of a packed bed of spheres on forced convection heat transfer from an embedded circular cylinder is investigated numerically under the *LTNE* assumption. The results show that Nu_f can be increased or decreased as d_p increases, depending on the values of k_d, Re_D, d_p, k_r, and h_{sf}. For example, for $Re_D \leqslant 10$, Nu_f decreases as d_p increases; however, for $Re_D > 40$, Nu_f increases as d_p increases depending on the dominance of the effect of k_d on that of K and k_{st} which is a direct function of k_r. Whereas, at a particular value of $Re_D = 40$, a decrease-increase trend of Nu_f is shown as d_p increases, which gives a clear depiction of competition between these effects on heat transfer. The influence of k_r on the trend of Nu_f versus d_p is found to be significant only at low $Re_D < 40$, also at $Re_D = 40$ when D_{cy}/d_p = 100–50, due to the weakness in the effect of k_d, otherwise, this influence diminishes. The results show that Nu_f decreases with increasing d_p at low $k_r \leqslant 1.0$, while it increases with increasing d_p at high k_r = 1000. Also, the results of the *LTNE* model is compared with those of the *LTE* model at different values of k_r and Re_D. Similar trend of results is obtained for both models at $k_r \leqslant 1.0$ for all Re_D; however, the models predict completely different trend of results at k_r = 1000, but only at the same low range of Re_D mentioned above. The comparison also concludes that the *LTE* model predicts Nu_f higher than that estimated by the *LTNE* one for $k_r \geqslant 1.0$, and the difference between their results for Nu_f increases as d_p decreases, or as Re_D, k_r, or h_{sf} increases. In addition, it is found that the presence of the porous medium enhances the overall heat transfer, but at the same time increases significantly the pressure drop in the bed. Interestingly, the results demonstrate that using spherical porous materials with larger diameter increases considerably the heat transfer and decreases greatly ΔP_f, which is the demand for any thermal application using porous media to enhance heat transfer.

References

[1] E. Achenbach, Heat and flow characteristics of packed beds, Exp. Therm. Fluid Sci. 10 (1) (1995) 17–27.
[2] B. Alazmi, K. Vafai, Constant wall heat flux boundary conditions in porous media under local thermal non-equilibrium conditions, Int. J. Heat Mass Transfer 45 (15) (2002) 3071–3087.
[3] A. Amiri, K. Vafai, Analysis of dispersion effects and non-thermal equilibrium, non-Darcian, variable porosity incompressible flow through porous media, Int. J. Heat Mass Transfer 37 (6) (1994) 939–954.
[4] A. Amiri, K. Vafai, Transient analysis of incompressible flow through a packed bed, Int. J. Heat Mass Transfer 41 (24) (1998) 4259–4279.
[5] A. Amiri, K. Vafai, T.M. Kuzay, Effects of boundary conditions on non-Darcian heat transfer through porous media and experimental comparisons, Numer. Heat Transfer (Part A) 27 (6) (1995) 651–664.
[6] N. Banu, D.A.S. Rees, Onset of Darcy–Benard convection using a thermal non-equilibrium model, Int. J. Heat Mass Transfer 45 (11) (2002) 2221–2228.
[7] A.C. Baytas, Thermal non-equilibrium natural convection in a square enclosure filled with a heat-generating solid phase, non-Darcy porous medium, Int. J. Energy Res. 27 (10) (2003) 975–988.
[8] A.C. Baytas, I. Pop, Free convection in a square porous cavity using a thermal nonequilibrium model, Int. J. Therm. Sci. 41 (9) (2002) 861–870.
[9] R.G. Carbonell, S. Whitaker, Heat and mass transfer in porous media, in: J. Bear, M.Y. Corapcioglu (Eds.), Fundamentals of Transport Phenomena in Porous Media, Martinus Nijhoff, Dordrecht, Boston, 1984, pp. 121–198.
[10] G. Chen, H.A. Hadim, Numerical study of three-dimensional non-Darcy forced convection in a square porous duct, Int. J. Numer. Methods Heat Fluid Flow 9 (2) (1999) 151–169.
[11] P. Cheng, Mixed convection about a horizontal cylinder and a sphere in a fluid-saturated porous medium, Int. J. Heat Mass Transfer 25 (8) (1982) 1245–1247.
[12] G.M. Chrysler, R.E. Simons, Experimental investigation of the forced convection heat transfer characteristics of fluorocarbon liquid flowing through a packed-bed for immersion cooling of microelectronic heat sources, in: Parallel and Vector Computation in Heat Transfer – Presented at AIAA/ASME Thermophysics and Heat Transfer Conference, Seattle, WA, USA, 1990, pp. 21–27.
[13] G.L. David, P. Cheng, A numerical solution of variable porosity effects on natural convection in a packed -sphere cavity, J. Heat Transfer 113 (1991) 391–399.
[14] F.A. Dullien, Media Fluid Transport and Pore Structure, Academic Press, New York, 1979.
[15] S. Ergun, Fluid flow through packed columns, Chem. Eng. Prog. 48 (2) (1952) 89–94.
[16] S.W. Hsiao, P. Cheng, C.K. Chen, Non-uniform porosity and thermal dispersion effects on natural convection about a heated horizontal cylinder in an enclosed porous medium, Int. J. Heat Mass Transfer 35 (12) (1992) 3407–3418.
[17] G.J. Hwang, C.H. Chao, Heat transfer measurement and analysis for sintered porous channels, Trans. ASME. J. Heat Transfer 116 (2) (1994) 456–464.
[18] D.B. Ingham, I. Pop, Transport Phenomenon in Porous Media, vol. 2, Pergamon, Oxford, 1979.
[19] U.A. Jeigarnik, F.P. Ivanov, N.P. Ikranikov, Experimental data on heat transfer and hydraulic resistance in unregulated porous structures, Teploenergetika 21 (1991) 33–38 (in Russian).
[20] P.X. Jiang, Z.P. Ren, Numerical investigation of forced convection heat transfer in porous media using a thermal non-equilibrium model, Int. J. Heat Fluid Flow 22 (1) (2001) 102–110.
[21] P.X. Jiang, Z.P. Ren, B.X. Wang, Z. Wang, Forced convective heat transfer in a plate channel filled with solid particles, J. Therm. Sci. 5 (1) (1996) 43–53.
[22] P.X. Jiang, G.S. Si, M. Li, Z.P. Ren, Experimental and numerical investigation of forced convection heat transfer of air in non-sintered porous media, Exp. Therm. Fluid Sci. 28 (6) (2004) 545–555.
[23] P.X. Jiang, B.X. Wang, D.A. Luo, Z.P. Ren, Fluid flow and convective heat transfer in a vertical porous annulus, Numer. Heat Transfer; Part A: Appl. 30 (3) (1996) 305–320.
[24] P.X. Jiang, B.X. Wang, Z.P. Ren, A numerical investigation of mixed convection in a vertical porous annulus, in: Proceedings of the 10th International Heat Transfer Conference, Brighton, UK, 1994, pp. 303–308.
[25] P.X. Jiang, Z. Wang, Z.P. Ren, B.X. Wang, Experimental research of fluid flow and convection heat transfer in plate channels filled with glass or metallic particles, Exp. Therm. Fluid Sci. 20 (1) (1999) 45–54.
[26] G.E. Karniadakis, M. Israeli, S.A. Orszag, High-order splitting methods for the incompressible Navier–Stokes equations, J. Comput. Phys. 97 (2) (1991) 414–443.

[27] M. Kaviany, Principles of Heat Transfer in Porous Media, Springer-Verlag, New York, 1995.
[28] S.M. Kuo, C.L. Tien, Heat transfer augmentation in a foam-material filled duct with discrete heat sources, in: InterSociety Conference on Thermal Phenomena in the Fabrication and Operation of Electronic Components, Los Angeles, CA, USA, 1988, pp. 87–91.
[29] A.V. Kuznetsov, A perturbation solution for heating a rectangular sensible heat storage packed bed with a constant temperature at the walls, Int. J. Heat Mass Transfer 40 (5) (1997) 1001–1006.
[30] A.V. Kuznetsov, Thermal nonequilibrium, non-Darcian forced convection in a channel filled with a fluid saturated porous medium – a perturbation solution, Appl. Sci. Res. 57 (2) (1997) 119–131.
[31] A.V. Kuznetsov, Thermal non-equilibrium forced convection in porous media, in: D.B. Ingham, I. Pop (Eds.), Transport Phenomena in Porous Media, Elsevier Science, Oxford, 1998, pp. 103–129 (Chapter 5).
[32] N.J. Kwendakwema, R.F. Boehm, Parametric study of mixed convection in a porous medium between vertical concentric cylinders, J. Heat Transfer 113 (1) (1991) 128–134.
[33] D.Y. Lee, K. Vafai, Analytical characterization and conceptual assessment of solid and fluid temperature differentials in porous media, Int. J. Heat Mass Transfer 42 (3) (1999) 423–435.
[34] W.J. Minkowycz, A. Haji-Sheikh, K. Vafai, On departure from local thermal equilibrium in porous media due to a rapidly changing heat source: the sparrow number, Int. J. Heat Mass Transfer 42 (18) (1999) 3373–3385.
[35] A.A. Mohamad, Nonequilibrium natural convection in a differentially heated cavity filled with a saturated porous matrix, J. Heat Transfer 122 (2) (2000) 380–384.
[36] K. Nasr, S. Ramadhyani, R. Viskanta, Experimental investigation on forced convection heat transfer from a cylinder embedded in a packed bed, J. Heat Transfer 116 (1) (1994) 73–80.
[37] D.A. Nield, Effects of local thermal non-equilibrium in steady convective processes in a saturated porous medium: forced convection in a channel, J. Porous Med. 1 (2) (1998) 181–186.
[38] D.A. Nield, A. Bejan, Convection in Porous Media, second ed., Springer Science+Business Media, New York, NY, USA, 2006.
[39] I. Pop, P. Cheng, Flow past a circular cylinder embedded in a porous medium based on the Brinkman model, Int. J. Eng. Sci. 30 (2) (1992) 257–262.
[40] M. Quintard, M. Kaviany, S. Whitaker, Two-medium treatment of heat transfer in porous media: numerical results for effective properties, Adv. Water Resour. 20 (2–3 special issue) (1997) 77–94.
[41] M. Quintard, S. Whitaker, One- and two-equation models for transient diffusion processes in two-phase systems, Adv. Heat Transfer 23 (C) (1993) 369–464.
[42] D.A. Rees, A.P. Bassom, I. Pop, Forced convection past a heated cylinder in a porous medium using a thermal nonequilibrium model: boundary layer analysis, Eur. J. Mech., B/Fluids 22 (5) (2003) 473–486.
[43] D.A.S. Rees, I. Pop, Vertical free convective boundary-layer flow in a porous medium using a thermal nonequilibrium model, J. Porous Med. 3 (1) (2000) 31–44.
[44] N.H. Saeid, Analysis of free convection about a horizontal cylinder in a porous media using a thermal non-equilibrium model, Int. Commun. Heat Mass Transfer 33 (2) (2006) 158–165.
[45] N.H. Saeid, I. Pop, Transient free convection in a square cavity filled with a porous medium, Int. J. Heat Mass Transfer 47 (8–9) (2004) 1917–1924.
[46] M.B. Saito, M.J. Lemos, Laminar heat transfer in a porous channel simulated with a two-energy equation model, Int. Commun. Heat Mass Transfer 36 (10) (2009) 1002–1007.
[47] M.C. Thompson, K. Hourigan, A. Cheung, T. Leweke, Hydrodynamics of a particle impact on a wall, Appl. Math. Model. 30 (11) (2006) 1356–1369.
[48] K. Vafai, Handbook of Porous Media, Marcel Dekker, New York, 2000.
[49] K. Vafai, M. Sozen, Analysis of energy and momentum transport for fluid flow through a porous bed, Trans. ASME J. Heat Transfer 112 (3) (1990) 390–399.
[50] N. Wakao, S. Kaguei, Heat and Mass Transfer in Packed Beds, Gordon and Breach, New York, 1982.
[51] N. Wakao, S. Kaguei, T. Funazkri, Effect of fluid dispersion coefficients on particle-to-fluid heat transfer coefficients in packed beds-correlation of Nusselt numbers, Chem. Eng. Sci. 34 (3) (1979) 325–336.
[52] B.X. Wang, J.H. Du, Forced convective heat transfer in a vertical annulus filled with porous media, Int. J. Heat Mass Transfer 36 (17) (1993) 4207–4213.
[53] J.H. Wang, H.N. Wang, A discussion of transpiration cooling problems through an analytical solution of local thermal nonequilibrium model, J. Heat Transfer 128 (10) (2006) 1093–1098.
[54] K.C. Wong, N.H. Saeid, Numerical study of mixed convection on jet impingement cooling in a horizontal porous layer under local thermal non-equilibrium conditions, Int. J. Therm. Sci. 48 (5) (2009) 860–870.
[55] W.S. Wong, D.A. Rees, I. Pop, Forced convection past a heated cylinder in a porous medium using a thermal nonequilibrium model: finite peclet number effects, Int. J. Therm. Sci. 43 (3) (2004) 213–220.
[56] P. Zehner, E.U. Schluender, Thermal conductivity of granular materials at moderate temperatures, Chem. Ing. Tech. 42 (14) (1970) 933–941.